Research Article | Vol. 7, No. 10 | 1 Oct 2016 | BIOMEDICAL OPTICS EXPRESS 4171

Biomedical Optics EXPRESS

All-optical highly sensitive akinetic sensor for ultrasound detection and photoacoustic imaging

STEFAN PREISSER,[1,2] WOLFGANG ROHRINGER,[1,2] MENGYANG LIU,[2] CHRISTIAN KOLLMANN,[2] STEFAN ZOTTER,[1] BALTHASAR FISCHER,[1] AND WOLFGANG DREXLER[2,*]

[1]*XARION Laser Acoustics GmbH, Ghegastraße 3, 1030, Vienna, Austria*
[2]*Center for Medical Physics and Biomedical Engineering, Medical University of Vienna, Währinger Gürtel 18-20, AKH 4L, 1090, Vienna, Austria*

[*]*wolfgang.drexler@meduniwien.ac.at*

Abstract: A novel all-optical akinetic ultrasound sensor, consisting of a rigid, fiber-coupled Fabry-Pérot etalon with a transparent central opening is presented. The sensing principle relies exclusively on the detection of pressure-induced changes of the refractive index in the fluid filling the Fabry-Pérot cavity. This enables resonance-free, inherently linear signal detection over a broad bandwidth. We demonstrate that the sensor achieves a exceptionally low peak noise equivalent pressure (NEP) values of 2 Pa over a 20 MHz measurement bandwidth (without signal averaging), while maintaining a flat frequency response, and a detection bandwidth up to 22.5 MHz (-6 dB). The measured large full field of view of the sensor is 2.7 mm × 1.3 mm and the dynamic range is 137 dB/$\sqrt{\text{Hz}}$ or 63 dB at 20 MHz bandwidth. For different required amplitude ranges the upper amplitude detection limit can be customized from at least 2 kPa to 2 MPa by using cavity mirrors with a lower optical reflectivity. Imaging tests on a resolution target and on biological tissue show the excellent suitability of the akinetic sensor for optical resolution photoacoustic microscopy (OR-PAM) applications.

OCIS codes: (170.0170) Medical optics and biotechnology; (170.5120) Photoacoustic imaging; (170.0110) Imaging systems; (170.0180) Microscopy; (170.7170) Ultrasound (040.0040); Detectors; (120.0120) Instrumentation, measurement, and metrology.

References and links

1. J. Yao and L. V. Wang, "Sensitivity of photoacoustic microscopy," Photoacoustics **2**, 87–101 (2014).
2. M. Xu and L. V. Wang, "Photoacoustic imaging in biomedicine," Rev. Sci. Instrum. **77**, 041101 (2006).
3. G. Ku, K. Maslov, L. Li, and L. V. Wang, "Photoacoustic microscopy with 2-μm transverse resolution," J. Biomed. Opt. **15**, 021302 (2010).
4. S. Hu, K. Maslov, and L. Wang, "Second-generation optical-resolution photoacoustic microscopy with improved sensitivity and speed," Opt. Lett. **36**, 1134–1136 (2011).
5. Z. Xie, S. Jiao, H. Zhang, and C. A. Puliafito, "Laser-scanning optical-resolution photoacoustic microscopy," Opt. Lett. **34**, 1771–1773 (2009).
6. J. Yao, L. Wang, J.-M. Yang, K. Maslov, T. Wong, L. Li, C.-H. Huang, J. Zou, and L. Wang, "High-speed label-free functional photoacoustic microscopy of mouse brain in action," Nat. Methods **12**, 407–410 (2015).
7. L. Xi, C. Song, and H. Jiang, "Confocal photoacoustic microscopy using a single multifunctional lens," Opt. Lett. **39**, 3328–3331 (2014).
8. J. Gateau, A. Chekkoury, and V. Ntziachristos, "Ultra-wideband three-dimensional optoacoustic tomography," Opt. Lett. **38**, 4671–4674 (2013).
9. C. Zhang, T. Ling, S.-L. Chen, and L. J. Guo, "Ultrabroad bandwidth and highly sensitive optical ultrasonic detector for photoacoustic imaging," ACS Photonics **1**, 1093–1098 (2014).
10. E. Zhang, J. Laufer, and P. Beard, "Backward-mode multiwavelength photoacoustic scanner using a planar Fabry-Pérot polymer film ultrasound sensor for high-resolution three-dimensional imaging of biological tissues," Appl. Opt. **47**, 561–577 (2008).
11. Z. Xie, S.-L. Chen, T. Ling, L. J. Guo, P. L. Carson, and X. Wang, "Pure optical photoacoustic microscopy," Opt. Express **19**, 9027–9034 (2011).

#273000 http://dx.doi.org/10.1364/BOE.7.004171
Journal © 2016 Received 2 Aug 2016; revised 7 Sep 2016; accepted 12 Sep 2016; published 19 Sep 2016

Biomedical Optics EXPRESS

12. H. Li, B. Dong, Z. Zhang, H. Zhang, and C. Sun, "A transparent broadband ultrasonic detector based on an optical micro-ring resonator for photoacoustic microscopy," Scientific Reports **4**, 4496 (2014).
13. H. Grün, T. Berer, P. Burgholzer, R. Nuster, and G. Paltauf, "Three-dimensional photoacoustic imaging using fiber-based line detectors," J. Biomed. Opt. **15**, 021306 (2010).
14. R. Nuster, H. Grün, B. Reitinger, P. Burgholzer, S. Gratt, K. Passler, and G. Paltauf, "Downstream Fabry-Pérot interferometer for acoustic wave monitoring in photoacoustic tomography," Opt. Lett. **36**, 981–983 (2011).
15. E. Khachatryan, S. Maswadi, D. A. Tsyboulski, E. Barnes, D. Sardar, A. A. Oraevsky, K. Nash, and R. Glickman, "Optoacoustic Microscopy Using Laser Beam Deflection Technique," Proc. SPIE **8943**, 89432T (2014).
16. B. Fischer, "Optical microphone hears ultrasound," Nat. Photon **10**, 356–358 (2016).
17. W. Rohringer, S. Preißer, M. Liu, S. Zotter, Z. Chen, B. Hermann, H. Sattmann, B. Fischer, and W. Drexler, "All-optical highly sensitive broadband ultrasound sensor without any deformable parts for photoacoustic imaging," Proc. SPIE **9708**, 970815 (2016).
18. B. Fischer, "Development of an optical microphone without membrane," Ph.D. thesis, Vienna University of Technology (2010).
19. D. Meschede, *Optics, Light and Lasers: The Practical Approach to Modern Aspects of Photonics and Laser Physics* (Wiley, 2007).
20. O. A. A. and A. A. Karabutov, "Ultimate sensitivity of time-resolved optoacoustic detection," Proc. SPIE **3916**, 386326 (2000).
21. A. M. Winkler, K. Maslov, and L. V. Wang, "Noise-equivalent sensitivity of photoacoustics," J. Biomed. Opt. **18**, 097003 (2013).
22. M. Jaeger, "Real-time optoacoustic imaging for medical diagnostics using linear array transducers," Ph.D. thesis, Philosophisch-Naturwissenschaftliche Fakultät, Universität Bern (2007).
23. S. A. Ermilov, T. Khamapirad, A. Conjusteau, M. H. Leonard, R. Lacewell, K. Mehta, T. Miller, and A. A. Oraevsky, "Laser optoacoustic imaging system for detection of breast cancer," J. Biomed. Opt. **14**, 024007 (2009).
24. B. E. Treeby and B. T. Cox, "k-Wave: MATLAB toolbox for the simulation and reconstruction of photoacoustic wave-fields," J. Biomed. Opt. **15**, 021314 (2010).
25. L. Li, C. Yeh, S. Hu, L. Wang, B. T. Soetikno, R. Chen, Q. Zhou, K. K. Shung, K. I. Maslov, and L. V. Wang, "Fully motorized optical-resolution photoacoustic microscopy," Opt. Lett. **39**, 2117–2120 (2014).
26. J. Liang, Y. Zhou, A. W. Winkler, L. Wang, K. I. Maslov, C. Li, and L. V. Wang, "Random-access optical-resolution photoacoustic microscopy using a digital micromirror device," Opt. Lett. **38**, 1683–2686 (2013).

1. Introduction

When pulses of laser light are delivered to biological tissues, some of that energy is absorbed inside the tissue and released as heat causing localized thermo-elastic pressure transients which can be detected by an ultrasonic transducer. By measuring these transients with an array, or by scanning the tissue surface with a single sensor, an image of the localized optical absorber can be visualized, referred to as photoacoustic imaging (PAI). The most commonly employed detectors for PAI are piezoelectric transducers which are readily available for a range of frequency bandwidths and sensitivities. However, piezoelectric transducers have physical limitations. First, there is an inherent tradeoff between element size and signal-to-noise ratio (SNR) [1]. While large piezoelectric transducers in principle offer low thermal noise and high sensitivity, their surface shape must be well matched to the pressure wavefront to allow a high numerical aperture (NA) for photoacoustic microscopy (PAM) [1, 2]. This can be achieved by employing focused transducers [3] or acoustic lenses [4]; however, both approaches limit the transducer's effective field of view (FOV) to the acoustic focal spot size, making mechanical scanning of the transducer necessary to cover the desired field of view. Mechanical scanning limits the frame rate in fast-scanning optical resolution photoacoustic microscopy (OR-PAM). Fast-scanning can be achieved with unfocused transducers [5] but without focusing the sensitivity is significantly reduced [1]. Because piezoelectric transducers are generally opaque, they cannot be placed in the optical path of the excitation laser, a further limitation for reflection mode OR-PAM systems. Mounting an unfocused transducer at an oblique angle with respect to the excitation beam path [5], is one way to address this problem but sacrifices SNR. An acoustic-optical beam combiner [4] can achieve fast scanning of both optical and acoustic focus with fast micro-electromechanical mirrors (MEMS) [6]. Unfortunately, large distances between microscope objective, transducer and sample are required for this approach. A third solution is using ring-shaped transducers with a central hole

Biomedical Optics EXPRESS

to allow transmission of the excitation beam [7]. These transducers are custom-made with different characteristics from piece to piece. If a transparent detector maintaining an SNR comparable to a focused transducer is available that would enable significantly simplified reflection-mode systems and facilitate the implementation of complementary imaging modalities, such as optical coherence tomography (OCT) or confocal microscopy.

Piezoelectric transducers rely on the detection of a mechanical deformation due to the strain induced by an ultrasound wave. This leads to a nonlinear frequency response peaked around a resonance frequency and limited bandwidth (BW). While broad-band detection can be achieved with polyvinylidene-fluorid-based (PVDF) hydrophones, for the most sensitive PZT transducers, the BW is typically on the same order of magnitude as the center frequency, resulting in narrow bandwidths, especially if highly sensitive detection of frequencies below 10 MHz is required. In photoacoustic imaging, artifacts are created by the simultaneous detection of small and large structures, where both high- and low-frequency spectral components are integrated for image reconstruction [8, 9]. Therefore, a sensor with a high sensitivity to low- and high-frequency spectral components would be best suited for PAI.

As an alternative to piezoelectric detectors, a number of different optical detection schemes have been developed in recent years. Examples are interferometric techniques such as polymer-membrane based Fabry-Perot interferometers (FPI) [10], optical micro ring resonators [11, 12], polymer fiber or fiber Bragg grating FPI [13], free-space interferometric techniques [14], and non-interferometric sensors [15]. While these address many of the outlined shortcomings, most of these techniques rely on the displacement of a mechanically deformable structure to generate the signal [10–13], which introduce self-resonances and therefore a frequency-dependent sensitivity.

This drawback can be avoided by measuring the refractive index change of a medium, which is directly related to the change of density when modulated by an acoustic wave. In PAT and PAM measurements with line detectors, a high sensitivity could already be realized with fiber-based sensors [13] or by using a free-space beam either in an interferometer setup [14] or in a deflection beam setup [15]. In the latter, the deflection of a probe beam inside a coupling fluid, caused by the refractive index change if the medium, was used to measure acoustic waves all-optically. The sensitivity of these measurement principles, however, are strongly dependent on the interaction cross section of the used probe beams with the acoustic wave. Therefore, these concepts cannot be easily miniaturized without loss of sensitivity. In addition, the spatial extent of the detection length increases the influence of other system parameters than pressure on the refractive index along the detection volume. These quantities, such as temperature, the piezo-optic coefficient of the coupling fluid or the speed of sound, can vary locally and can also change in time during the duration of a measurement, leading to sensitivity shifts and spurious contributions to the signal which may be hard to correct for.

Here, we present a miniaturized all-optical akinetic detector based on a rigid Fabry-Perot (FP) resonator without deformable parts which can achieve outstanding sensitivity, a large FOV, a flat frequency response up to 22.5 MHz (-6 dB) and optical transparency.

2. All-optical akinetic sensor and its detection principle

The detection principle of the akinetic sensor is outlined in Fig. 1(a). It has already been successfully applied for ultrasound detection [16, 17] and for acoustic sensing in different media and frequency regimes [18]. The intensity reflected from a FP cavity is given by the product of the input intensity I_0 and a transfer function $TF(q)$, which for an ideal resonator, is given by the Airy function [19]

$$TF\,(q) = 1 - \frac{1}{1 + F \cdot \sin\left(\frac{q}{2}\right)^2}, \tag{1}$$

Biomedical Optics EXPRESS

with the finesse coefficient $F = 4R/(1-R)^2$, where R denotes the mirror reflectivity. The round trip phase shift q depends on the laser wavelength λ, the mirror distance d and the refractive index n of the medium between the cavity mirrors as

$$q(n) = \frac{4\pi n d}{\lambda}. \tag{2}$$

In contrast to membrane, piezoelectric, or fiber-based optical sensors, where the ultrasound wave displaces a deformable mechanical structure, effecting a change of the geometric length d of the resonator, in case of the all-optical akinetic sensor a rigid FP cavity is placed so that the ultrasound wave passes through the medium located between the resonator mirrors. Since the wave constitutes a change of the medium's density, and thereby its refractive index n, the optical path length $n \cdot d$ between the resonator mirrors is altered. The resulting shift of the cavity resonance can be probed with a narrow-linewidth detection laser (center wavelength 1550 nm) stabilized to the inflection point of the Airy function Fig. 1(a). The resulting change of the reflected light intensity I is measured with a photodiode, a low noise amplifier and a fast digital acquisition card.

To achieve high sensitivities, the change of intensity for a given shift of the cavity resonance with respect to the detection laser needs to be maximized. A measure for this quantity is the cavity bandwidth, representing the FWHM width of the resonance:

$$BW_{FWHM} = \frac{FSR}{\mathcal{F}(R)} = \frac{c}{2nd\mathcal{F}(R)}. \tag{3}$$

Here, FSR denotes the free spectral range of the resonator in units of frequency, $\mathcal{F}(R)$ the cavity finesse (which only depends on reflectivity), and c the speed of light in vacuum. It is apparent from Eq. 3 that the cavity bandwidth, and therefore the sensitivity of the all-optical sensor is determined by the distance between mirrors and the finesse. Hence, for resonators with different mirror distances, identical sensitivities can be achieved in practice by choosing mirror reflectivity accordingly, and there is no inherent performance penalty for miniaturization, which is not the case for piezoelectric transducers [20, 21].

Figure 1(b) contains a sketch of the sensor head. The acoustic wave passes through a transparent central opening of ~ 2 mm by 2 mm, the biggest dimension has an extension of ~ 6 mm, and a thickness of 1 mm. Since the sensor head is machined as a rigid structure, mechanical deformation can be neglected, so that the signal is only contributed by the change of the refractive index n, yielding an akinetic detection mechanism. Note that the exact geometry and size can be adapted to different target applications, and that sensors of various shapes and sizes have been realized. The detection laser is coupled to the cavity via an optical fiber and suitable beam shaping optics to provide the needed beam profile. The beam diameter of 60 µm and the mirror distance of 2 mm define the active detection volume of the sensor. Note that for these small beam diameters, diffraction is not negligible and may reduce the effective finesse of the resonator. Hence, the mirror surface needs to be matched to the wavefront to achieve highest sensitivities. The frequency response is also mainly determined by the beam diameter. In the following, we neglect beam divergence and assume propagation of the ultrasound field along the direction x, oriented orthogonally with respect to the detection laser axis. Then, the normalized response of the detector can be calculated using a one-dimensional convolution between the Gaussian-shaped beam profile with fixed beam radius w_0 and sine functions representing each frequency component of the pressure field:

$$P_m(k) = \int_{-\infty}^{\infty} p_s(k) \sin\left(k(x-x')\right) \cdot \exp\left(-\frac{2x^2}{w_0^2}\right) \cdot dx'. \tag{4}$$

Here, $p_s(k)$ denotes the pressure amplitude at the location of the sensor for each frequency com-

Biomedical Optics EXPRESS

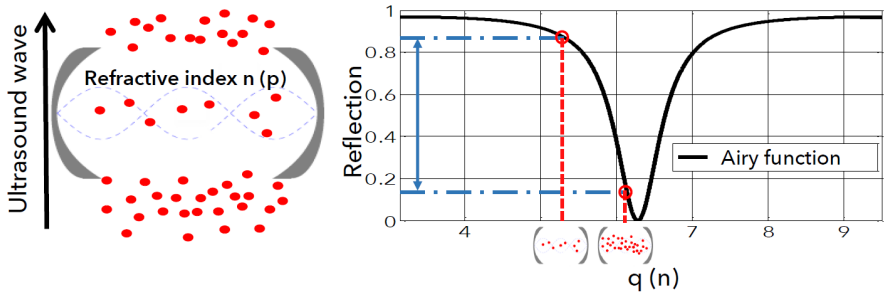

(a)

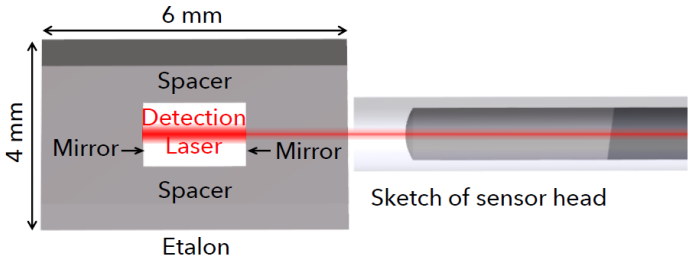

(b)

Fig. 1. (a) Detection principle of the akinetic sensor. A pressure wave constitutes a density change in the medium (illustrated by the red dots) between the resonator mirrors, altering the optical pathlength via a change of the refractive index n. This leads to a resonance shift, which can be detected by monitoring the light intensity reflected by the resonator. (b) Sketch of the sensor head and detection volume (detection laser diameter of 60 µm and mirror diameter of 2 mm).

ponent, and $P_m(k)$ the corresponding measured amplitude. Physically, for acoustic wavelengths smaller than the beam diameter, the detector averages over volumes with high and low pressure, and the detected signal decreases, whereas, as long as the wavelength is larger than the beam diameter, in good approximation a flat frequency response is expected. A comparison between measurement and a numerical evaluation of Eq. 4 is shown in section 4.1.

In addition, the line-shaped detection volume offers another significant advantage over piezoelectric transducers. The signal amplitude from an unfocused, planar piezo transducer is significantly influenced in many ways by the angle of incidence of the pressure transient. The two most important points are: first, piezoelectric material has an angular sensitivity, since the charge induced by the pressure transient depends on the direction of the mechanical stress. The sensitivity to the normal stress component κ_n is normally much higher than to the shear (transverse) stress component κ_τ. Second, if the wavelength of the ultrasound wave is smaller than the piezoelectric element, the signal depends on the overlap of the transient and the piezo element [22]. The signal received by a transducer $P_{tr}(r,\theta,t)$ can therefore be described by [23]:

$$P_{tr}(r,\theta,t) = \frac{v_s}{L}(\kappa_n sin\theta + \kappa_\tau cos\theta)\frac{r_0}{r}\int_{t-0.5\alpha(\theta)}^{t+0.5\alpha(\theta)} p_0^{'}(t)dt, \tag{5}$$

where $p_0^{'}(t)$ is the pressure amplitude at the source, r_0 is the initial radius at the source, with the speed of sound v_s, the temporal interval $\alpha(\theta) = Lcos(\theta)/v_s$ and L the width of the transducer. A signal received by a planar transducer at an incident angle θ (angle between the acoustic

Biomedical Optics EXPRESS

wave vector and the surface of the transducer) will therefore be averaged over the temporal interval $\alpha(\theta)$, and weighed by the factor $cos\theta$. A large aperture provides high sensitivity for planar transients traveling perpendicular to the aperture area, whereas only a spatially averaged pressure is detected from transients incident under an oblique angle $\theta < 90°$. In the application of photoacoustic microscopy, the ultrasound generating absorbers are small compared to the width of single element transducers, and thus the wavefront is in good approximation spherically. Therefore, without wavefront matching of the transducer (focused transducer), the sensitivity is decreased. In addition, for small distances, not the full aperture is exposed to mechanical stress and the output signal is reduced since it is generated as the average pressure inside the whole transducer element. Therefore, sensitivity is decreased when measuring small spherical waves typically generated in PAM.

While this effect is also present for the all-optical sensor, it is much less pronounced, since in contrast to the piezoelectric transducer, where the pressure field is integrated over an area, here the integration is performed along a line. As an example, the signals generated by the akinetic sensor and a flat transducer with an active area of 4 mm × 4 mm, both placed at a distance of 1 mm from the source of a spherical pressure wavefront can be simulated with the k-Wave toolbox [24]. For the all-optical detector, the pressure was averaged over an effectively line-shaped detection volume with 2 mm length and 60 µm diameter, reproducing the experimental parameters. Simulation results for a pressure signal with 15 MHz center frequency show that averaging over the active area of the planar sensor reduces the measured signal amplitude by a factor of 100 with respect to the actual pressure amplitude, while for the optical sensor, the measured signal is only reduced by a factor of 5. These simulations and measurement results shown in section 4.3 illustrate that providing acoustically focused detection is much less critical for the optical sensor than for a piezoelectric transducer, if the sensor can be placed close to the sample.

To achieve good acoustic coupling to water or biological tissue, the cavity is filled with a low optical absorbing fluid enabling good acoustic impedance match to water. The encapsulation is realized by a thin foil with a thickness of <25 µm. The sensor may be immersed into a water bath or coupled to the sample with a drop of water or a thin layer of ultrasound gel. Tests with the sensor immersed into liquid with and without foil did not show any effect of the encapsulation on the sensitivity and frequency response within the measurement BW.

3. Setup of acoustic detector characterization

Measurements of the frequency response, directional response, dynamic range and sensitivity of the optical sensor were carried out by using the substitution method where alternately the all-optical akinetic sensor and a needle hydrophone as a reference were used to measure the acoustic field. This reference was a calibrated PVDF membrane needle hydrophone (Acoustic Precision) with an active element diameter of 1 mm. Four different piezo transducers were used as acoustic sources with 1 MHz (Panametrics V303-SU), 5 MHz (Panametrics V326-SU), 10 MHz (Panametrics V311-SU) and 25 MHz (Panametrics V324-SU) center frequencies, as well as 80 % BW (Olympus Panametrics) to cover the whole frequency range of the optical sensor. Using transducers of large active element size and measuring the acoustic waves in the far field leads to an approximately uniform wavefront, which can be considered a plane wave at length scales comparable to the sensor diameter. The sensor and the calibrated hydrophone where mounted on an electronically controlled scanning stage, allowing independent translation in the X, Y, and Z directions with a step size of 250 µm. The rotation around the vertical axis was performed by a rotation mount (see Fig. 2(a)). The calibrated hydrophone and the optical sensor were aligned on the same axis of rotation, which was particularly important for the directivity measurements. In addition to the piezo transducers, a photoacoustic source was used to determine the sensitivity, enabling a direct comparison of the SNR of the optical sensor and commercially available piezo transducers.

Biomedical Optics EXPRESS

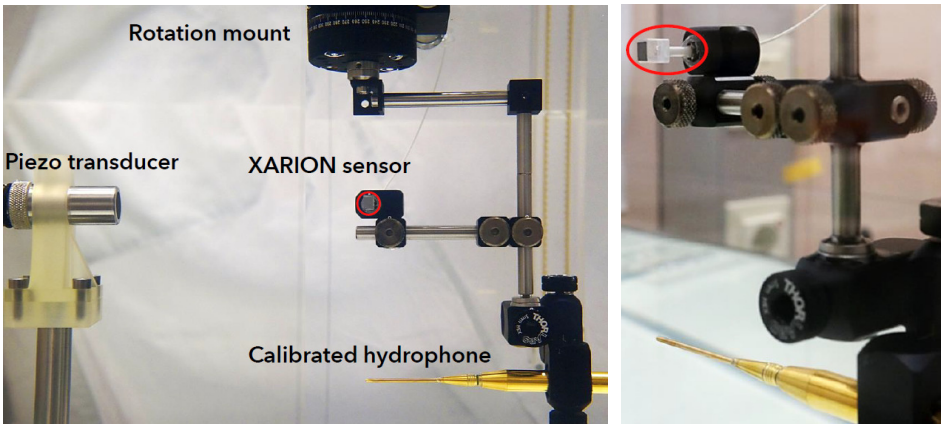

(a) (b)

Fig. 2. Photograph of the acoustic characterization set-up. (a) Measurement set-up submerged in water. The calibrated needle hydrophone (Acoustic Precision) and the all-optical akinetic sensor (marked by a red circle) are mounted in the axis of the rotation mount. PZT transducers function as sound sources. Distances in the photograph has been adapted for demonstration purpose to better show the entire setup. (b) Zoomed-in photograph of the measurement setup under a different angle showing the all-optical sensor marked by a red circle.

4. All-optical akinetic sensor characterization

Unless otherwise stated, all characterization measurements reported in this section were obtained with the substitution setup explained in section 3.

4.1. Frequency response

In order to measure the frequency response of the all-optical akinetic sensor, the discrete Fourier transformation was used both on the recorded time domain waveforms measured by the calibrated needle hydrophone and the all-optical akinetic sensor. The hydrophone measurements were then corrected according to the frequency response of the calibrated needle hydrophone (calibration curve). Subsequently, the corrected curve was compared to the frequency curve measured by the optical sensor thus obtaining the frequency response. Four different piezo transducers as acoustic sources were necessary to cover the frequency range from 0.5 MHz to >25 MHz.

Biomedical Optics EXPRESS

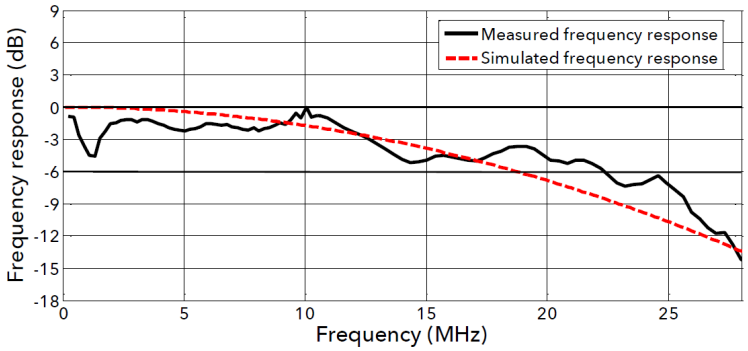

Fig. 3. Measured frequency response of the all-optical akinetic sensor plotted as a solid black line and the simulated frequency response using Eq. 4 plotted as a dashed red line.

The normalized frequency response of the optical sensor is shown in Fig. 3. It can be seen that the response covers a 22.5 MHz BW (-6 dB). The measured frequency response (black solid line) corresponds well to the theoretically predicted curve (red dashed line) of the optical sensor calculated from Eq. 4. At the cutoff frequency of 25 MHz, the ultrasound wavelength is equal to the detection laser diameter of 60 µm. For acoustic wavelengths smaller than the beam diameter, the detector averages along the detection laser beam with high and low pressure, and the detection sensitivity decreases, which can be seen in Fig. 3.

4.2. Directional response

The directional response of the optical hydrophone was obtained by rotating it through 180° in steps of 1° in the acoustic far field generated by piezo-electric transducers. For a line detector, it can be assumed that the directional response of the sensor is not isotropic in three dimensions, but should show two varying angular response characteristics depending on the spatial angle between the acoustic wave and the detection laser beam. For a planar wavefront, two cases have to be addressed: one, where the arriving wavefront is parallel to the laser, and one, where there is an angle between the wavefront and the laser. Based on the rotational symmetry of a line detector, the directivity in the first case should be omnidirectional and only disturbed by the thin glass body of the sensor. In the second case, the sensor should be highly directional for oblique incidence of sound waves with respect to the detection laser. The sensitivity drop in the second case is based on the fact that the path length of interaction between the acoustic wave and the detection volume expands with an increasing deviation from a normal incidence angle. Therefore, the detector averages over volumes with high and low pressure, and the detected signal decreases due to the same mechanism responsible for the upper frequency response cutoff mentioned in section 4.1.

Biomedical Optics EXPRESS

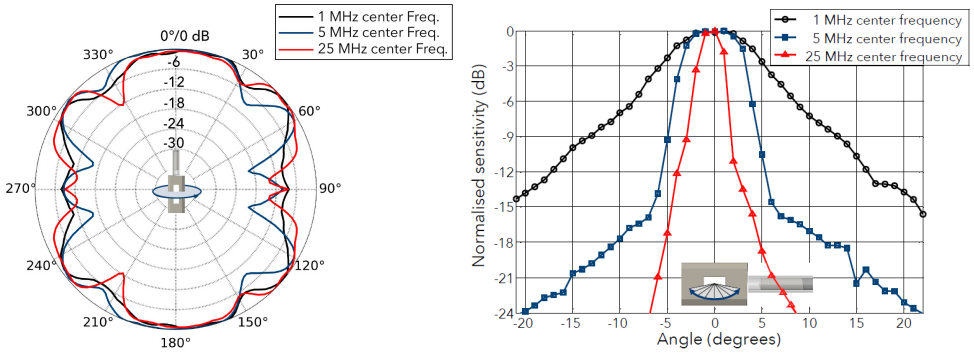

(a) (b)

Fig. 4. Directional responses of the akinetic sensor. (a) The polar pattern shows a flat directional response for rotation parallel to the detection laser axis. (b) Directive response for higher frequencies for rotation of rotating the sensor orthogonal to the detection laser axis.

Therefore, the directional response for the two orthogonal planes were measured separately. Using three different PZT transducers, we were able to obtain the two directional responses as a function of frequency. The results for the first case (normal incidence of the wavefront with respect to the detection laser) are shown in Fig. 4(a). In the polar pattern, an almost flat directional response can be seen. The rotational symmetry is interrupted by recurring acoustic shadowing due to the glass body of the sensor when it is between the transducer and the detection laser (for example at 35°). Due to acoustic diffraction, the signal is not completely attenuated but by a factor of -12 dB . In the second case the angular sensitivity depends strongly on the acoustic frequency, as can be seen in the measurement results shown in Fig. 4(b). The sensor shows a directive response in this measurement axis.

4.3. Sensitivity

To characterize the sensitivity, we determined the noise equivalent pressure (NEP) of the all-optical sensor by measuring the ratio A_s/N_{RMS} in a photoacoustic tomography setup, as outlined below. Here, A_s denotes the single-sided peak amplitude of the photoacoustic signal, and N_{RMS} the root mean square (RMS) noise amplitude within a frequency bandwidth Δf in the absence of a pressure signal. If both quantities are known in terms of pressure units, A_s denotes the NEP, if the ratio A_s/N_{RMS} is unity. It was determined by direct comparison of the maximum peak amplitudes and RMS noise amplitudes measured by the optical sensor and the calibrated PVDF needle hydrophone. A typical signal trace measured with the optical sensor is included in the inset of Fig. 5(a). In order to measure the RMS noise values, background signals were recorded in the absence of an excitation laser for photoacoustic signal generation. Normalizing the measured voltage values of the PVDF hydrophone to the calibration sensitivity (1607 mV/MPa), absolute pressure values at the position of the hydrophone could be determined. For an optimized sensor, this comparison gave a NEP of 450 µPa/$\sqrt{\text{Hz}}$ at 1 MHz, corresponding to 2 Pa normalized to a 20 MHz measurement BW. In figure 5(a), the fundamental NEP limits for PZT-based transducers in relation to the sensor aperture diameter is shown, based on theoretical models for thermal noise found in literature [20, 21]. The NEP values determined for the optical sensor lie below these theoretical limits for the relevant aperture diameter of 2 mm and are within a factor of two of the theoretical self noise limits for commercially available focused piezo transducers (e.g. Olympus V324-SM, 6.35 mm active element diameter).

Biomedical Optics EXPRESS

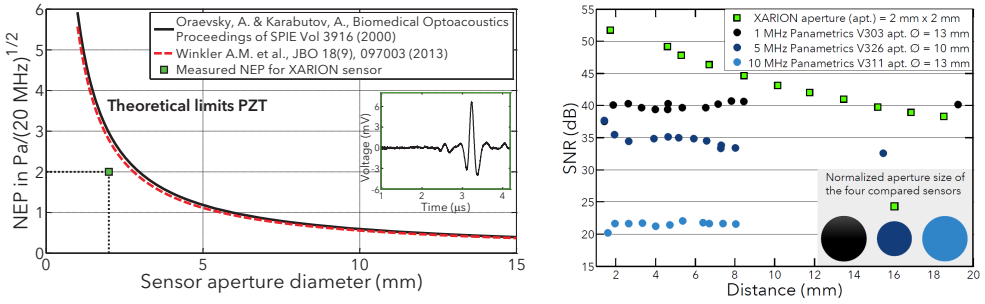

(a) (b)

Fig. 5. Sensitivity results. (a) Measured noise equivalent pressure of the all-optical akinetic sensor, compared to theoretical limits due to thermal noise for piezoelectric transducers. The characterized test sensor outperforms piezo-electric transducers of identical element size. (b) Signal-to-noise measurements of the akinetic sensor, compared to Olympus piezo-electric transducers. Frequency range of the ultrasound source was between 0.5 MHz and 3.5 MHz (-6 dB).

For a direct comparison between PZT piezoelectric transducers and the all-optical akinetic sensor we measured the SNR for each sensor measuring photoacoustic generated pulses. The excitation source, a pulsed Nd:YAG laser (Quanta-Ray PRO-270-50, Spectra-Physics) was coupled into a fiber with a core diameter of 1.5 mm and irradiated a PTFE-Tubing filled with a mixture of India-ink and water. The India-ink serving as an optical absorber within the mixture resulting in an absorption coefficient of $\mu_a = 0.2\,\mathrm{mm}^{-1}$ generated an ultrasound pulse in the frequency band of 0.5 MHz to 3.5 MHz verified by the calibrated needle hydrophone.

By measuring the peak signal amplitude and the RMS noise amplitude in the absence of a pressure signal, the SNR was determined depending on the distance between the tubing and the all-optical sensor for three different Panametrics transducers (V303, V326, V311). The signals of both types of sensors were amplified by a low-noise amplifier (DHPVA Femto, Germany) to guarantee that the measured noise is not dominated by the data acquisition system. The SNR comparison (Fig. 5(b)) shows a considerably higher SNR for the optical sensor when placed close to the tubing and followed by a decreasing SNR when enlarging the distance. That behavior is caused by decreased sound amplitudes for longer distances between source and sensor, due to geometric spreading, whereas the noise floor is not affected by the distance change. In comparison, the signal amplitude measured by an unfocused, planar transducer decreases significantly with decreasing distance from the source of a cylindrical wavefront generated from the tubing, since the wavefront is not matched to the active area of the planar transducers.

Furthermore, if the sensor is placed close to the tubing, only a fraction of the surface is hit by the ultrasound waves and only a small part of the surface is able to generate a signal whereas the remaining surface does not participate to signal generation. Since the total signal output is generated as a mean amplitude value over the whole surface, the signal diminishes by averaging. Considering these two facts, which reduce the measured signal near small sources and counteract the increase of pressure amplitude close to the source, it can be seen in Fig. 5(b) that changing the distance between the tubing and the large area transducers has only minimal effect on the measured SNR in contrast to the all-optical akinetic sensor findings.

These measurements show that not only the NEP values of different sensors are important for an SNR comparison, but also the wavefront matching, which depends strongly on the dimension, form and distance of the source to the sensor. On the other hand, the line-shaped detection volume of the all-optical sensor prevents severe loss of SNR caused by averaging over areas with

Biomedical Optics EXPRESS

high amplitudes and areas with low amplitudes, because the sensor is small compared to the spacial expansion of the measured ultrasound waves generated from the tubing. In contrast to piezoelectric transducers, where sensitivity drops if the size is reduced, the all-optical sensor does not have this limitation. Therefore, the advantage of the optical sensor compared to transducers is its size, since it can be used to achieve even further gains in SNR compared to piezoelectric transducers with identical NEP by simply placing the optical sensor closer to the source. This is supported by another advantageous feature of the sensor, its insensitivity to illumination with excitation light.

4.4. Dynamic range and upper detection limit

In order to achieve a wide amplitude range for the all-optical ultrasound detector to address different needs on the detection limits, two all-optical sensors were built. In addition to the high finesse FP cavity sensor used for the measurements shown previously, one with a lower finesse FP cavity was also built for higher amplitude ranges.

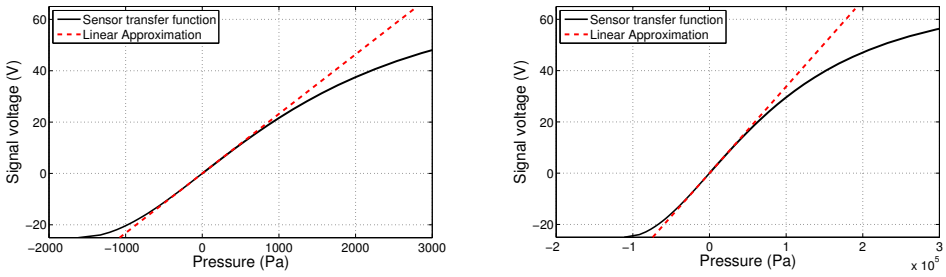

Fig. 6. (a) Interferometer transfer function of the high sensitive sensor. (b) Interferometer transfer function of the optical sensor with a extended upper detection limit

In figure 6(a), the transfer function for the high finesse FP cavity sensor with a 25 MHz BW and a 2 Pa NEP is shown. It can be seen that an almost linear measuring range is given to an upper limit of 2 kPa, and the dynamic range can therefore be calculated for a 20 MHz BW to be 60 dB or, in reference to a 1 Hz BW, 133 dB/$\sqrt{\text{Hz}}$. To reach a wider amplitude range the transfer function of the second sensor has a smoother slope (see Fig. 6(b)) and therefore a higher NEP of 45 Pa, determined in the same manner as for the high sensitive sensor. The upper linearity limit is at 200 kPa and the dynamic range can be calculated for a 25 MHz BW to be 73 dB or 147 dB/$\sqrt{\text{Hz}}$.

5. Photoacoustic biomedical application of the all-optical akinetic sensor

To demonstrate the applicability of the all-optical sensor for PAI, we used it to perform imaging of biological samples. To this end, a transmission mode OR-PAM setup was modified to allow integration of the all-optical sensor instead of the focused transducer typically employed for detection. A sketch of the setup is shown in Fig. 7(a). By using this setup, the mounting of the all-optical akinetic sensor was implemented in transmission mode, as can be seen in Fig. 7(b).

Biomedical Optics EXPRESS

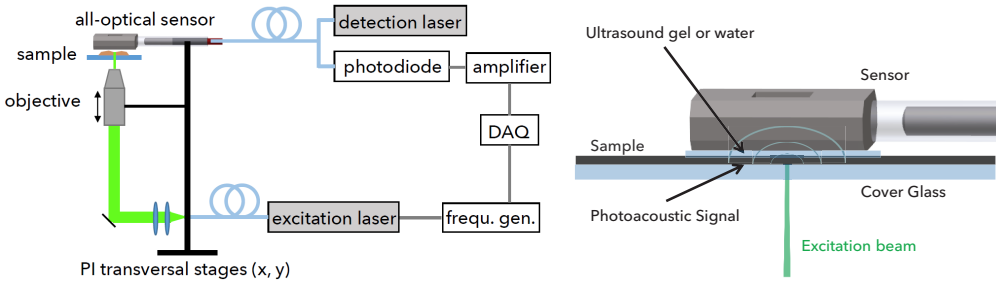

Fig. 7. (a) Sketch of the PAM setup. (b) Mounting of the sensor in the transmission-mode OR-PAM setup.

One feature of the all-optical sensor is that it can be used both in transmission mode and in reflection mode without any significant loss in SNR. This was verified by a sensitivity comparison measurement with a black plastic foil, one measurement in transmission mode and one in reflection mode (foil mounted above the sensor), showing no SNR differences (data not shown here). During imaging, the detector was acoustically coupled by a drop of water or a layer of ultrasound gel to the sample from above. The opening of the sensor was positioned in such a way that the sample was centered right below. The excitation light featured a wavelength of 532 nm by means of a Q-switched diode-pumped Nd:YAG laser (ElforLight, SPOT-10-200-532). The pulse durations of a few ns and pulse energies up to 1 µJ measured after the output of a single mode fiber was delivered, at a repetition frequency of 10 kHz. A 10x (Olympus) objective with a numerical aperture of 0.25 was applied for the US Air Force (USAF) resolution target and the red blood cells measurements, and a 4x long working distance objective (Olympus) with numerical apertures of 0.1 for the zebrafish and Feulgen-stained Allium Cepa histology samples. The focused beam was scanned in x and y dimensions by scanning the microscope objective by two orthogonally placed translation stages (PI, M-511 DD2) featuring a minimal step size of 100 nm. Unless noted otherwise, the detector was moved together with the microscope objective, while the sample was mounted in a fixed position. This was due to the fact that the setup was initially designed using a focused piezoelectric transducer in mind, where mechanical displacement of the sensor is necessary due to a small field of view of 50 µm.

Biomedical Optics EXPRESS

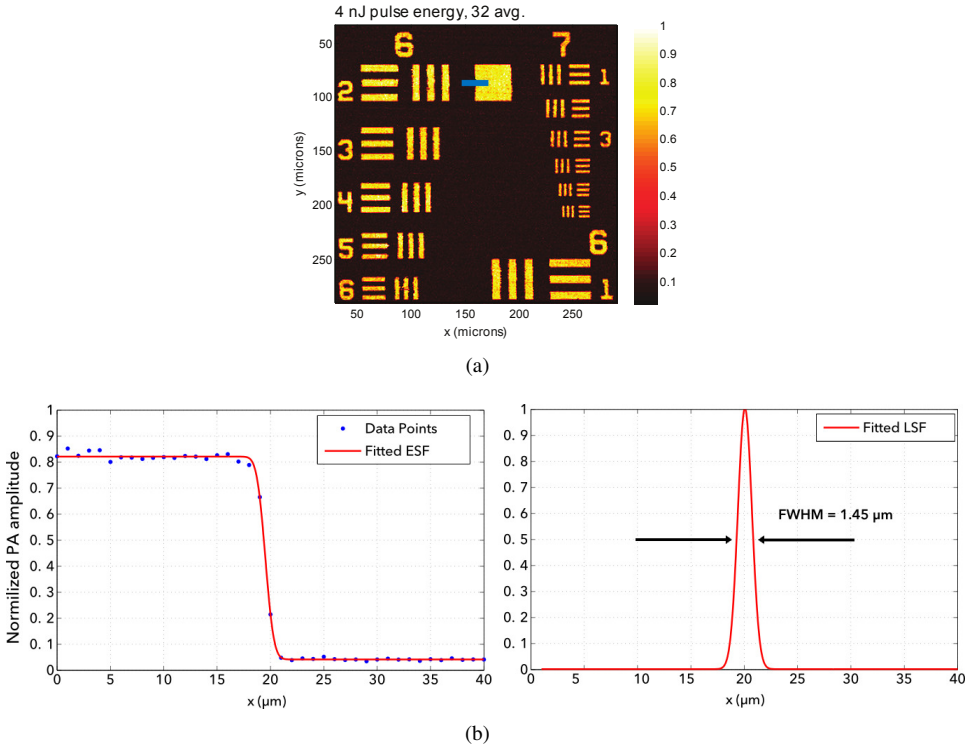

Fig. 8. (a) OR-PAM image of the central region containing the smallest groups 6 and 7 of a USAF resolution test target using a pulse energy of 4 nJ with a 10x objective. (b) The edge of the chrome rectangle was scanned illustrated by the blue line in (a) providing the step-edged function. The ESF was well fitted and the FWHM of the derived LSF represents the lateral resolution of the system. With the 10x Olympus objective lens (NA 0.25), the lateral resolution was measured as 1.45 μm, and R2 value, the goodness of fit, was 0.9993.

For the purpose of measuring the lateral resolution of the system the 10x Olympus objective was used. We verified the resolution by applying the step-edge method [25]. For this method a sharp-edged object is imaged for the experimental quantification of the imaging system resolution. In our case the edge of the rectangle chrome of the USAF resolution target shown in Fig. 8(a) was scanned in 100 nm steps in x direction and 400 nm steps in y direction (edge illustrated with a blue line). The edge-spread function (ESF) was estimated by measuring the edge response (mean value of 40 individual edge scans along the y direction), and was fitted to an error function,

$$\mathrm{f(x)} = A \cdot \mathrm{erf}\left(\frac{-x + x_0}{c \cdot \sqrt{2}}\right) + d, \tag{6}$$

assuming that the beam profile was Gaussian (see Fig. 8(b)). The line-spread function (LSF) was then calculated by differentiating the ESF. The resolution of the imaging system, defined by the full width at half maximum (FWHM) of the LSF, was thus derived for the 10x objective to be 1.45 μm (see Fig. 8(b)) which is near the abbe diffraction limit of 1.3 μm.

Biomedical Optics EXPRESS

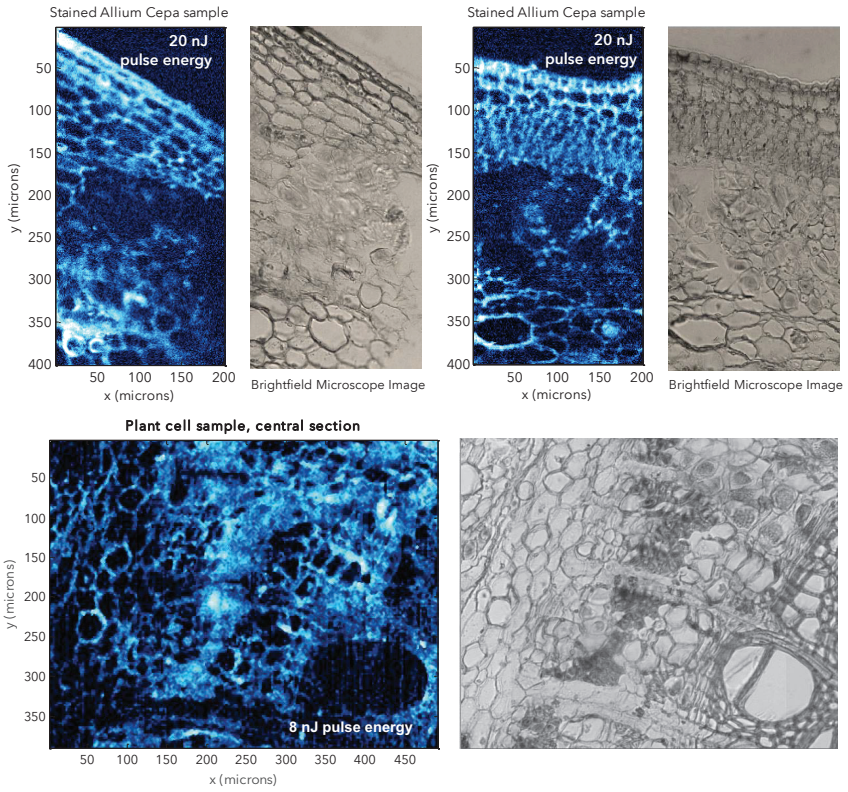

Fig. 9. Comparison of OR-PAM (blue) and brightfield microscope images of Feulgen-stained Allium Cepa histology samples. For the images in the upper panel, a pulse energy of 20 nJ was used, while for the picture in the lower panel, the pulse energy was reduced to 8 nJ, demonstrating the possibility of performing imaging on biological tissue with low fluence, although the sensor is not focused.

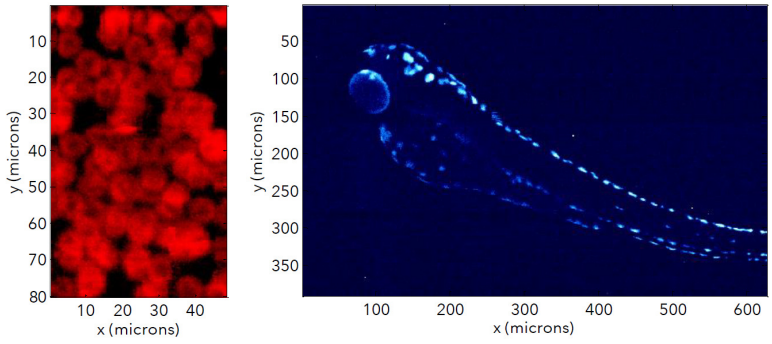

(a) (b)

Fig. 10. (a) OR-PAM image of red blood cells of a mouse imaged with pulse energies of 10 nJ. (b) OR-PAM image of an *ex vivo* zebra fish embryo imaged with pulse energies below 15 nJ.

Biomedical Optics EXPRESS

The low NEP determined in characterization measurements, together with the line-shaped detection volume which allows to maintain high SNR even without focused detection, is expected to enable the use of low pulse energies. As a demonstration, Fig. 8(a) shows an image of a USAF resolution target (Thorlabs), where the 10x microscope objective and a pulse energy of 4 nJ were used.

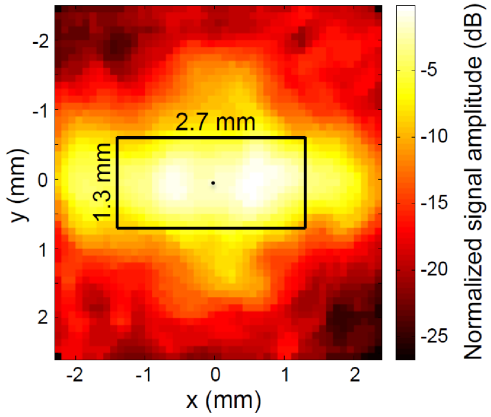

Fig. 11. Field of view covered by the all-optical sensor at 4.5 mm distance between detection laser and sample. For this measurement, the sensor was kept at a fixed position, while the excitation laser was grid-scanned over a piece of black plastic foil with homogeneous absorption. The measured wide FOV of 2.7 mm by 1.3 mm, is defined by the positions where the normalized photoacoustic signal drops by 6 dB with respect to the maximum recorded signal amplitude. A small black dot in the center symbolizes the FOV of a highly sensitive focused piezoelectric transducer and serves for comparison.

As an application-relevant example using biological tissue, Fig. 9 depicts sections of a histology sample containing Feulgen-stained Allium Cepa cells. OR-PAM images are shown in blue color, while brightfield microscope pictures are given in grayscale for comparison. Images in the upper panels were recorded using a pulse energy of 20 nJ, while the lower panel demonstrates that pulse energies below 10 nJ can be employed not only for the USAF resolution target, but also for stained histology samples. Further imaging examples with pulse energies below 15 nJ are given in Fig. 10(a) and 10(b), showing red blood cells of a mouse as well as the typical pigmentation of an *ex vivo* zebra fish embryo, respectively.

Fast-scanning methods for OR-PAM rely on lasers with high repetition rates, matched by rapid deflection of the excitation laser, mostly via galvanometer mirrors, digital micromirror devices [26], or most recently, MEMS mirrors [6], allowing scan frequencies of several tens of kHz. In such a scenario, mechanical displacement of the sensor is not an option. Figure 11 shows a measurement of the wide FOV covered by the optical sensor, which enables PAM without the necessity of mechanical scanning. To perform this measurement, the excitation laser was scanned over the surface of a piece of black plastic foil with homogeneous absorption, while the detector stayed at a fixed position on top of the foil, with a distance between detection laser and a sample of 4.5 mm. The figure contains a plot of the SNR as a function of the displacement of the excitation laser with respect to the center of the sensor. It shows that the change of SNR is smaller than 6 dB within a 2.7 mm by 1.3 mm. For comparison, the field of view determined by the focal spot size of a typical 25 MHz focused transducer (Olympus V324-SM) is approximately 50 µm. In conclusion we found the all-optical akinetic sensor to be excellently suited for fast scanning OR-PAM setups.

Biomedical Optics EXPRESS

6. Conclusion

We have presented a novel, akinetic, transparent all-optical sensor for ultrasound detection and photoacoustic imaging. Characterization measurements show that the detection principle allows broadband detection with a flat frequency response up to 22.5 MHz. Higher frequencies are detected with reduced sensitivity. The directional response measurements show an omnidirectional response and a very directive response depending on the rotation axis relative to the detection laser axis. Furthermore, we could show that it is possible to adjust the detectable ultrasound amplitude ranges to required values, changing the reflectivity of the cavity mirrors. NEP of as low as 2 Pa related to a 20 MHz BW, was measured by comparison of signal amplitudes and RMS noise values of the all-optical sensor with a calibrated hydrophone. Latest results with an improved photo detector give genuine hope that NEP values below 1 Pa in a 20 MHz BW should be feasible in the very near future. Furthermore, we could show that the optical sensor technology based on line detection is suitable for the detection of ultrasound with various wave shapes with a high sensitivity without the need of wavefront shaping for example with acoustic lenses, by k-wave simulations and SNR comparison measurements between our all-optical akinetic sensor and unfocussed piezo transducers. In addition, the light absorption of the sensor in the visible and NIR spectra is negligible which enables the sensor to be used near the sample in photoacoustic imaging without generating a photoacoustic wave inside the sensor itself leading to a high SNR.

In order to show that these results are reflected in the capability of performing OR-PAM using low pulse energies, imaging tests in a transmission OR-PAM setup were performed. The FOV was measured to cover a 2.7 mm by 1.3 mm area at 4.5 mm distance between sensor and sample.

The demonstrated features are expected to be highly useful for various different imaging applications. An especially promising route to be explored in the near future is the implementation of a highly sensitive, combined fast-scanning reflection mode OR-PAM + OCT multimodal setup, integrating photoacoustic microscopy with complementary morphology information from OCT at high imaging speed.

In addition to PAM, the sensor is well suited for applications where the hydrophone is mechanically stressed, since the sensor consists of a rigid FP without any membrane that could be damaged by high ultrasound amplitudes. This is in contrast to needle hydrophones, for instance, where large pressure amplitudes may affect the calibration or even destroy the membrane.

Furthermore, we will concentrate on suppressing the diffraction effects on the directional response and reducing the optical pathway through the opening of the sensor by suitable sensor geometries. Thereby the FOV could be extended, and a combination with other imaging modalities could be simplified. Additionally, further miniaturization of the sensor will open up endoscopy applications, where highly sensitive detection of small element size is of particular importance.

Funding

Austrian Research Promotion Agency (FFG BRIDGE) (848463); European Union (FAMOS) (FP7 ICT, 317744).

Acknowledgments

We thank Dr. Hannah Schneeweiss for providing plant histology samples and Dr. med. univ. Chengjing Zhu for the RBC samples used in application tests. Sensors and test equipment were provided by XARION Laser Acoustics GmbH.